

LAGRANGE: A Space-Based Gravitational-Wave Detector with Geometric Suppression of Spacecraft Noise

Mission Concept: Interferometry between three non-drag-free spacecraft in a geometry suppressing non-gravitational effects offers substantial science at significantly reduced cost and risk.

We are willing to participate and present the concept at a workshop.

This document has been cleared for unlimited release under the number URS225851

Lead Author: Kirk McKenzie (kirk.mckenzie@jpl.nasa.gov, Phone: (818) 235 8358)¹,

Co-Authors: Robert E. Spero¹, William M. Klipstein¹, Glenn de Vine¹, Brent Ware¹, Michele Vallisneri¹, Curt Cutler¹, John Ziemer¹, Daniel A. Shaddock², Ruth Skoug³, and John Steinberg³

¹Jet Propulsion Laboratory, California Institute of Technology, Pasadena, California

²Department of Physics, The Australian National University, Canberra, Australia

³Los Alamos National Laboratory, Los Alamos, New Mexico

November 10, 2011

Abstract

We introduce a new non-drag-free concept for space-based gravitational wave detection in which the spacecraft constellation geometry is chosen so the largest spacecraft disturbances are weakly coupled into the science measurement, and existing instruments are used to calibrate these effects. A three spacecraft constellation is presented with significant hardware simplifications and reductions in spacecraft mass, power, and size compared with the Laser Interferometer Space Antenna (LISA) mission, while preserving much of the LISA science (see Figure 1). The cost is estimated to be \$ 1.1 Billion (FY12 dollars).

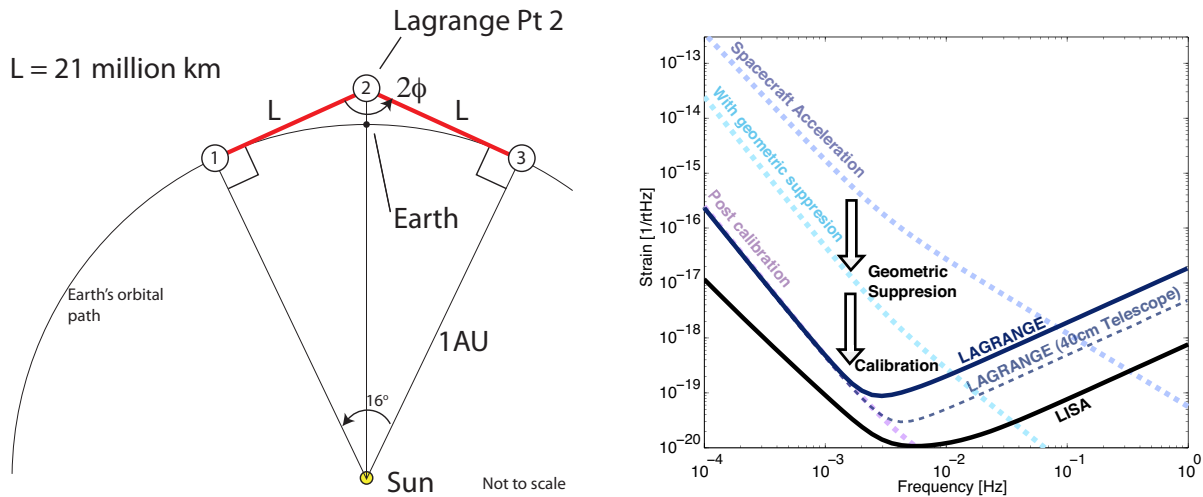


Figure 1: Left: Geometric suppression of spacecraft noise: solar-radiation and solar-wind pressures are orthogonal to the interferometer sensitive axis. Right: While degraded from the LISA sensitivity, this mission is sensitive enough to retain much of the science.

1 Introduction

This paper introduces a concept for a space-based laser interferometer gravitational-wave detector that, like the Laser Interferometer Space Antenna (LISA) [1], uses precision laser interferometry between widely

separated (millions of kilometers) spacecraft. The mission concept, which we call LAGRANGE, departs from LISA significantly in the hardware required on each spacecraft and their orbits. Where LISA uses a specialized drag-free system to isolate the proof masses (the measurement fiducial for the strain measurement) from external instrument noise, LAGRANGE will have the spacecraft itself as the fiducial for the measurement, following other previous non-drag-free mission concepts [2, 3]. Fluctuating forces on spacecraft at 1 AU (Astronomical Unit) cause spacecraft displacement noise that is many orders of magnitude too large to detect gravitational radiation without noise mitigation. We rely on two ideas to substantially reduce spacecraft displacement noise in the final science measurement:

1. Design of the spacecraft orbits to provide a geometric suppression of external spacecraft forces in the interferometer measurement direction. We expect a geometric suppression factor of 100 of radial solar-derived forces can be achieved.
2. Directly measure external spacecraft forces to 1% in the Sun's radial direction and calibrate their effect in the final science measurement. This performance is consistent with existing sensors. (The calibration accuracy without geometric suppression would have to be 0.01%.)

The largest spacecraft disturbances in the LISA frequency band are caused by fluctuating solar radiation pressure and fluctuating solar wind pressure. These forces act in a direction approximately radially out from the Sun, inviting a spacecraft constellation to minimize the coupling of these disturbances into the sensitive direction. The spacecraft (S/C) constellation, shown schematically in Figure 1 (left), was designed explicitly to suppress radial acceleration noise, while maintaining the initial constellation geometry. The lengths of the arms and the internal angle of the Michelson interferometer are set by the requirement of achieving geometric suppression of spacecraft noise. The end spacecraft (S/C 1 and S/C 3) are in circular heliocentric orbit in the plane of the ecliptic at 1 AU and lead/trail the Earth by $\theta = 8^\circ$, while the middle spacecraft (S/C 2) is in a small Lissajous orbit about the second Lagrange point ($\mathcal{L}2$) of the Sun-Earth system. Dual one-way interferometer links between the end and middle spacecraft will be employed so a Michelson interferometer combination can be formed with S/C 2 at the center. The separation of the end spacecraft about the Earth was chosen so that the normal vector to the radial direction of each spacecraft intersects at $\mathcal{L}2$, where S/C 2 is located. Ideally, this leads to perfect geometric suppression of radial acceleration noise on the end spacecraft. Moreover, the radial acceleration noise on the middle spacecraft is common to both arms of the Michelson configuration and therefore will cancel to a high level. For the nominal orbits presented here, the arm lengths are $L = L_{12} = L_{23} = 2.1 \times 10^{10}$ m, about 4 times larger than LISA's, and the angle between the Michelson arms is $2\phi = 164^\circ$. Orbital dynamics cause the constellation to drift over the 2 year mission life, breaking the perfect geometrical suppression of radial noise. However, a geometric suppression factor of 100 or more is maintained throughout the mission.

The solar-wind and solar-radiation pressure remain as the largest sources of spacecraft displacement noise, despite the reduction due to geometry. These will be reduced further in post-processing by subtracting calibrated measurements of each force. Force measurements could be derived from instruments based on those previously flown e.g. the SWEPAM solar wind monitor [4, 5] and the VIRGO radiometer [6, 7].

An estimate of the strain sensitivity of LAGRANGE is shown in Figure 1 (right). While the LAGRANGE constellation was set to minimize the spacecraft noise coupling into the interferometer link, the telescope size (20 cm diameter) and other interferometer components were chosen in an effort to minimize the size of the spacecraft and the cost of the mission. The sensitivity is limited by residual solar wind fluctuations at low frequencies ($f < 2$ mHz) and by optical shot noise above this. The sensitivity is reduced in comparison to the LISA science requirement at all frequencies: a factor of 20 at 100 μ Hz; a factor of 5 at 2 mHz; and a factor of 25 at frequencies above this. While the total science return is lessened, we expect that many of the sources observable by LISA will also be seen by this mission, albeit with reduced rates of detection. LAGRANGE will attain the fundamental scientific objectives to explore the physics of black

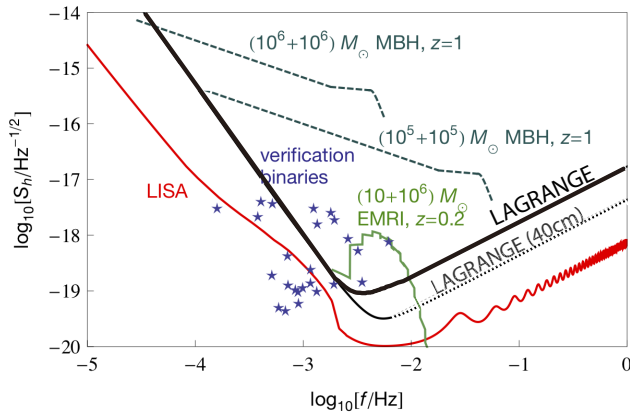


Figure 2: LAGRANGE (black) and LISA (red) rms strain. Roughly speaking, all sources above a missions noise curve are detectable by that mission. Blue stars represent the frequencies and strength of known Galactic binaries; their height above the noise curve gives their matched-filtering signal-to-noise ratio (SNR) in a one-year integration. Dashed grey curves and the solid green curve represent sources (two MBH binaries, and an EMRI, respectively) whose frequency evolves upward significantly during Lagranges observation time. The height of the source curve above the noise strain approximates the SNR contributed by each logarithmic frequency interval.

holes, and advance understanding of the fundamental physics of the universe, laid out by the Astro2010 Decadal Review [8], and adopted by NASA.

LAGRANGE offers potential for considerable reductions in hardware complexity, cost, and risk. The removal of the LISA drag-free system (the gravitational reference system (GRS) and the micro-Newton thrusters) yields a reduction in risk and spacecraft requirements, and build tolerances can be relaxed, including self-gravity and stray magnetic fields. Lower power consumption allows a smaller solar panel and a smaller spacecraft diameter. Finally, we estimate the simplicity of this mission will yield substantial cost and risk reductions compared to the LISA mission. Significant savings in hardware and operations are achieved, with an expected total cost of \$1.1 Billion, based off costing of other LISA-like missions [9].

2 Science

Figure 2 gives a snapshot comparison of LAGRANGE and LISA sensitivity to various fiducial, astrophysical sources. The LAGRANGE noise curve is plotted for two values of the telescope diameter: 20 cm (solid black curve - called LAGRANGE) and the 40 cm (dashed curve - referred to as LA40). A one-sentence summary is that LAGRANGE and LA40 could fulfill most of the LISA science objectives, though with decreased accuracy, increased risk of zero EMRI detections, and significantly decreased potential for discovering unforeseen sources or probing new physics. In more detail, both LAGRANGE and LA40 would detect 6 known verification binaries [10], and would resolve $\sim 10,000$ detached binaries and 1400 Am CVns. These numbers are all comparable to what one would observe with LISA; compared to LISA, for Galactic binaries, LAGRANGE's main drawback is that its decreased sensitivity at high frequency means that there are many fewer binaries measured, diminishing its ability to reveal details of mass transfer. Also, LAGRANGE (LA40) would detect an estimated 17 (20) MBH binary mergers per year, with 3 (5) of them having $SNR > 100$. This is 40% (60%) of the estimated detection rate for LISA, and so, like LISA, LAGRANGE would help trace the formation, growth and merger history of MBHs. The very closest, highest-SNR MBH binaries would confront General Relativity by providing a comparison of the highly accurate, observed merger/ringdown waveform (so in the highly relativistic, nonlinear regime) with the prediction from numerical relativity; however, the noise-induced errors in the LAGRANGE (LA40) measurement would be a factor 10 (3) worse than LISA's due to LAGRANGE's larger noise. LAGRANGE (LA40) would detect an estimated 5 (100) EMRIs per year, out to $z \sim 0.07$ (0.2). EMRI signals last for years, and the observed waveforms contain of order 100,000 cycles. This huge number of cycles, and the resulting sensitivity of the GW signal to small changes in source parameters, imply that LAGRANGE would typically measure the mass and spin of the MBH, as well as the mass of the inspiraling compact object, all to fractional accuracy $\sim 0.01\%$. For the same reason, every discovered EMRI provides an exquisite test of General Relativity, and of the null hypothesis that the central massive objects in galactic nuclei are truly black holes (as opposed to, say, very massive boson stars).

However our best estimates of the EMRI event rate is still rather poorly constrained by existing data and simulations, and could certainly be too optimistic by a factor of ~ 100 . Therefore for LA40 there is a modest risk that no EMRIs at all would be observed, and for LAGRANGE that risk is significant.

As mentioned above, descopeing from LISA to LAGRANGE has perhaps its greatest effect on the mission's discovery potential. The principal reason is the decrease from 6 laser links to 4. With only 4 links, only a single Time-Delay Interferometry (TDI) observable can be constructed. With only one observable, a stochastic GW background would be very difficult to distinguish from some unexpected source of instrumental noise. By comparison, 6-link LISA permits the construction of 3 independent TDI observables, from which one can independently estimate the magnitudes of both the instrumental noise and the GW noise from the early universe. Similarly, consider the case of searches for GW bursts; e.g., the case of bursts from cosmic (super-) strings, which have a characteristic (roughly) sine-Gaussian shape. Detected in only one channel, it would be difficult to have great confidence that the burst was not some instrumental artifact. But with either 5 or 6 links, one could measure both components of polarization, which would provide a powerful veto against non-GW bursts.

3 Mission Description

The LAGRANGE mission is based heavily on the LISA mission. Summarized in Table 1, it consists of three widely separated spacecraft in heliocentric orbit with four one-way inter-spacecraft optical links. Each spacecraft is designed to support the scientific payload that consists of the interferometer measurement system (IMS) and the spacecraft force measurement (SFM) instruments. The two end spacecraft have one IMS and one set of SFM instruments, while the middle spacecraft has two IMS and one set of SFM instruments. The IMS and the SFM instruments will record data, which will be decimated and sent to Earth periodically. This data will be combined in post-processing.

3.1 Interferometer Measurement System

LAGRANGE shares many components of the interferometric measurement system with LISA: the phase measurement chain; laser frequency noise control; ultra stable optical path length. However, stability requirements on many of these components can be relaxed by a factor of 16 as shot noise, the dominant interferometric noise, is approximately 16 times higher than on LISA (a factor of 4 relaxation because of the arm length, and a factor of 4 because we choose a smaller telescope diameter, single link displacement noise of $146 \text{ pm}/\sqrt{\text{Hz}}$ for LAGRANGE compared with $8.6 \text{ pm}/\sqrt{\text{Hz}}$ for LISA). At the same time, some demands on the IMS are more stringent than on LISA: the light power will be 250 times less than for LISA and the Doppler shifts (heterodyne frequency) will be up to 6 times larger.

Phase Measurement System: Conceptually, the phase measurement chain – photoreceivers, analog-to-digital converters, and phasemeters – that make up the phase measurement system could remain largely unchanged from those already developed for LISA. The reduced light power and larger Doppler shifts (heterodyne frequency) motivate wider bandwidth and higher gain photoreceivers and faster processing electronics (by a factor of 4). These additional requirements may be accommodated with minor modifications and the relaxation of the displacement requirements.

Laser Frequency Control and Ultra-Stable Oscillator Noise Cancellation: Laser frequency control and ultra-stable oscillator noise cancellation will be performed in the same manner as LISA, using laser pre-stabilization via arm locking [11], and Time Delay Interferometry (TDI) [12, 13]. For cost and complexity reductions we have removed on-board laser stabilization in favor of arm locking alone, which has been shown to meet the pre-TDI requirements on LISA [14, 15, 16].

Table 1: LAGRANGE Mission Parameters

Predicted Event Rates and Event Numbers		
Frequency band	100 μ Hz to 0.1 Hz	
Massive black hole mergers	15 yr^{-1} to 25 yr^{-1} , 2-5 with SNR > 100	
Extreme mass ratio inspirals	10 M_{\odot} + 10 ⁶ M_{\odot} pair seen out to $z = 0.1$	
Detectable verification binaries	6, (with SNR > 5).	
Galactic binaries	10000 detached binaries yr^{-1} and 1400 Am CVns yr^{-1}	
Mission		
Science measurement	Michelson interferometer phase change induced by incident gravitational radiation	
Duration	2 years science operation (4 years including transfer and commissioning)	
Orbits	Three spacecraft: S/C 1 (S/C 3) in 8° Earth leading (trailing) heliocentric orbit, S/C 2 in orbit around the 2nd Lagrange Point of the Sun-Earth system.	
Optical Links	Dual one-way interferometer links between S/C 1 and 2, and between S/C 2 and 3.	
Spacecraft bus	Provides power, communication. Reaction wheels for attitude control and hydrazine desaturation thrusters. Power supply from solar cells.	
Propulsion module	Used for orbit insertion, chemical propulsion. Mass, Power.	
Constellation	Isosceles triangle: Central S/C at 2nd Lagrange point, end S/C at two other vertices. Internal angle at central S/C is 164°, and arm lengths are 2.1×10^{10} m. At end S/C, interferometer link direction is at normal to Sun's radial direction to receive geometric suppression of solar forces. Arm lengths $\pm 5\%$, central S/C angle $\pm 0.1^\circ$, rel. S/C velocity < 100 m/s, geometric suppression > 120	
Total mass	2820 kg, including LV adapter	
Power per S/C	450 W	
Spacecraft Radius	0.9 m	
Data volume	60 Mbit/day per spacecraft (0.3 Hz interferometer data rate).	
Launch vehicle	Falcon 9, Block 3	
Instruments		
<i>Attitude Control: < 100 μrad between attitude correction maneuvers.</i>		
Reaction Wheels	4 per S/C	GRAIL-like reaction wheels (TBC).
Desaturation Thrusters	3 clusters per S/C	Hydrazine propulsion system
<i>Spacecraft Force Measurement. Single link acceleration : $a(f) \approx 2.5 \times 10^{-16} \times (1\text{Hz}/f)^{3/4} \text{ m/s}^2/\sqrt{\text{Hz}}$</i>		
Solar Wind Monitor	1 per S/C	SWEPAM-like [4]
Radiometer	1 per S/C	VIRGO-like radiometer [6]
Accelerometer	1 per S/C	GOCE-like [19]
<i>Interferometric Measurement System: Single link displacement : $x(f) \approx 150 \text{ pm}/\sqrt{\text{Hz}}$</i>		
Interferometry	Heterodyne interferometry 150 $\text{pm}/\sqrt{\text{Hz}}$ level, inter-S/C ranging to 1 m, clock noise transfer	
Laser	2 (S/C 1, 3), 4 (S/C 2)	1.2 W, wavelength 1064 nm, frequency stability (free-running) 30 $\text{kHz}/\sqrt{\text{Hz}} \times (1\text{Hz}/f)$, fractional power stability $10^{-4}/\sqrt{\text{Hz}}$
Optical Bench	1 per S/C	Fused silica optics bonded to a Zerodur Bench
Telescope	1 (S/C 1, 3), 2 (S/C 2)	20 cm diameter. Fixed telescope pointing.
In-field guiding mirror	2 (middle S/C only)	Michelson internal angle variation $\pm 0.15^\circ$
Phase measurement system	1 per S/C	
Point ahead mirror	No actuation	1 μ rad offset (in plane only), ± 10 nrad variability.

3.2 Force measurement system

The SFM departs significantly from LISA's GRS. Rather than isolating the proof mass (the measurement fiducial for LISA), this mission uses instruments to measure the parameters that lead to the forces on the spacecraft, and uses this data to subtract the effect of the forces in post-processing. We envisage the SFM

to consist of three instruments: a solar wind monitor, a radiometer, and an accelerometer. Each instrument will make measurements in the radial direction: with the solar wind monitor and radiometer measuring parameters related to the solar wind pressure and solar radiation pressure respectively, while the accelerometer will make a direct measurement of the acceleration of the spacecraft. While three instruments are surplus to correct for two forces, the accelerometer can be used as a redundant sensor and can be used to provide an absolute calibration for the solar pressure forces.

Solar wind monitor: A solar wind monitor on each spacecraft will measure the speed, direction, and density of the solar wind at a rate of 0.1 Hz. These data will be transmitted to the ground where the resulting force on the spacecraft will be calculated. The performance of previously flown solar wind monitors, such as the SWEPAM instrument, appears to be sufficient to calculate the force of the solar wind applies on the spacecraft to a precision of 1% (see Appendix B).

Radiometer: The solar radiation on each spacecraft will be measured with sufficient precision to enable subtraction of the resulting spacecraft acceleration noise. The DC component of the solar radiation pressure on the spacecraft is approximately 1000 times the fluctuating component in a 1 Hz bandwidth [17, 18]. The radiometer flown on the SOHO mission has sufficient noise performance and dynamic range to enable more than a factor of 100 reduction of radiation pressure fluctuations, enough to reduce radiation pressure well below the LISA acceleration noise budget.

Accelerometer: We propose to use an accelerometer like the ONERA accelerometer [19] used on the GOCE mission in concert with the radiometer and the solar wind monitor. The accelerometer noise performance is $a_{acc}(3 \text{ mHz}) = 3 \times 10^{-12} \text{ m/s}^2/\sqrt{\text{Hz}}$ and it has sufficient dynamic range of $3 \times 10^6 / \sqrt{\text{Hz}}$ to measure the solar fluctuations without drag compensation. The accelerometer could be used to provide a absolute calibration of acceleration of the radiometer and solar wind monitor and additional diagnostics.

3.3 Spacecraft Impact

The removal of the LISA drag-free system yields several benefits. The spacecraft build requirements are lessened: self-gravity and stray magnetic fields are less of a concern. We estimate 340 kg of reduction per spacecraft is possible. Since the drag-free system including thrusters use significant power, spacecraft power (approximately 350 W in total) is reduced, thus decreasing the size of the solar panels and lowering mass. The complexity of the interferometer on the bench is lessened, as no proof mass interferometry is needed.

3.4 Measurement Concept

The measurement and calibration of noise sources in the interferometer link can be illustrated by considering only the acceleration noise of the spacecraft due to solar radiation pressure fluctuations and assume this force noise acts precisely radially from the Sun. If the face of the spacecraft is aligned precisely with the radial direction, the resulting acceleration noise will also be purely radial. We label the acceleration noise of the j th spacecraft facing the i th spacecraft $\hat{a}_{ij}(t) = \alpha_{ij}(t)\mathbf{a}_{ij}$ with $\alpha_{ij}(t)$ the magnitude of the acceleration and \mathbf{a}_{ij} a unit vector describing the direction of the acceleration. The acceleration noise in individual links are given by $s_{ij} = (\hat{a}_{ij}(t) - D_{ij}\hat{a}_{ji}(t)) \cdot \hat{n}_{ij}$, where \hat{n}_{ij} is a unit vector describing the direction of propagation of the interferometer link and D_{ij} is the delay operator defined $D_{ij}a(t) = a(t - L_{ij}/c)$ [20]. The acceleration noise in the interferometer link between S/C 1 and S/C 2 is $s_{12}(t) = a_{12}(t) - D_{21}a_{21}(t) \sin \Delta\theta$, where $\Delta\theta$ is the deviation of the angle subtended by the radial direction at S/C 1 and the interferometer link between S/C 1 and S/C 2 from 90° (a maximum of 0.6° for the orbits considered here). Thus, the first order coupling of acceleration noise of S/C 1 into this interferometer link is suppressed by a minimum of 100. Next, we propose to measure the radiation pressure fluctuations in the radial direction using a radiometer. Then this measurement will be used to subtract the disturbance from the interferometer measurement channels. The measurement of the apparatus on S/C j can be converted to acceleration $\alpha_{mj}(t) = \alpha_{ij}(t) + \alpha_{Nj}(t)$, where $\alpha_{Nj}(f)$ is the underlining noise floor of the measurement apparatus. This measurement is scaled by $\sin \Delta\theta$

to cancel the S/C acceleration noise from the interferometer channels. The result is a calibrated measurement

$$s_{12|CAL} = s_{12}(t) - \alpha_{m1}(t - L/c) \sin \Delta\theta = \hat{a}_{12}(t) - \alpha_{N1}(t - L/c) \sin \Delta\theta \quad (1)$$

showing the residual noise of S/C 1 is limited by the noise floor of the acceleration noise measurement apparatus scaled by $\sin \Delta\theta$. Thus, the result is a reduction of apparatus noise over using the same apparatus to measure the acceleration in the sensitive direction. This reduction of apparatus noise moves the noise performance of existing instruments into the performance required for LISA type sensitivities. Of course, the acceleration noise of S/C 2 remains in equation 1. But the radial component of this noise is common to both arms of the Michelson interferometer and cancels to a high level when the Michelson combination is formed, as shown in Appendix A. Note that we do not assume that the acceleration noise is correlated between spacecraft, nor assume any common mode rejection factor.

4 Acceleration Noise Estimates and Detector Sensitivity

Starting with the magnitude and direction of the spacecraft acceleration noise (left, Figure 3), the expected noise that couples into the Michelson interferometer (center, Figure 3) is reduced by the constellation geometry. Finally, we perform the expected subtraction of the force noise to give the acceleration noise in the science observable (right, Figure 3).

4.1 Spacecraft acceleration noise

The acceleration noise of the spacecraft is up to 30,000 times larger than the LISA proof mass requirement [21, 22]. These forces are estimated using a combination of data and expected design parameters. Table 2 and Figure 3 (left) summarize the expected acceleration noise of each spacecraft. All calculations assume the expected force is converted into acceleration of the spacecraft using the area of the spacecraft facing the Sun: 3 m^2 and the spacecraft mass: 300 kg (Note: our estimated mass is 450 kg). In addition to the magnitude estimate in Table 2, the component that is in the radial and transverse direction is estimated.

Solar radiation is radial to a very good approximation and we estimate a negligible transverse component due to this, including consideration of coupling through S/C pointing. However, the solar wind direction varies significantly with almost zero mean, a Gaussian-like distribution, and standard deviation of $\sigma = 3^\circ$. To calculate the coupling into the interferometer link we assume $\theta_{SW} = 2\sigma$ as a conservative assumption of the noise coupling, thus 95% of the time the noise coupling will be smaller. Acceleration noise through difference in the thermal radiation of the front and back of the spacecraft is calculated assuming the following parameters: the spacecraft temperature is 300 K, the spacecraft surfaces transverse to the interferometer sensitive axis can be stabilized or measured to $10 \text{ mK}/\sqrt{\text{Hz}}$, and the sides of the spacecraft aligned with the sensitive direction to $0.1 \text{ mK}/\sqrt{\text{Hz}}$.

Table 2: Spacecraft forces

Acceleration Source	Acceleration Magnitude [$\text{m}/\text{s}^2/\sqrt{\text{Hz}}$]	Radial Component	Transverse Component	Notes
Solar Radiation Pressure	$a_{RP} = 6.8 \times 10^{-11} \times \left(\frac{1\text{mHz}}{f}\right)^{\frac{1}{3}}$	a_{RP}	0	Reference [17, 18]
Solar Wind Pressure	$a_{SW} = 1.0 \times 10^{-13} \times \left(\frac{1\text{Hz}}{f}\right)^{3/4}$	$a_{SW} \cos \theta_{SW}$	$a_{SW} \sin \theta_{SW}$	3 year average [4]
Thermal Radiation	$a_{Th} = 2.0 \times 10^{-12}$	a_{Th}	$a_{Th} \left(\frac{A_S}{A_F} \frac{\delta T_S(f)}{\delta T_F(f)}\right)$	Estimate
Lorentz Force	$a_{LF} = 5 \times 10^{-19} \times \left(\frac{1\text{Hz}}{f}\right)$	a_{LF}	a_{LF}	B-field data from [4], 10V S/C potential
Laser Intensity Recoil	$a_{IR} = 1.1 \times 10^{-15}$	0	a_{IR}	Estimate

4.2 Acceleration Noise Coupling into the Michelson Interferometer

The acceleration noise budget for the Michelson combination, X , shown in Figure 3 (center), is formed by combining measurements from the four optical links with appropriate delays. From the difference in noise

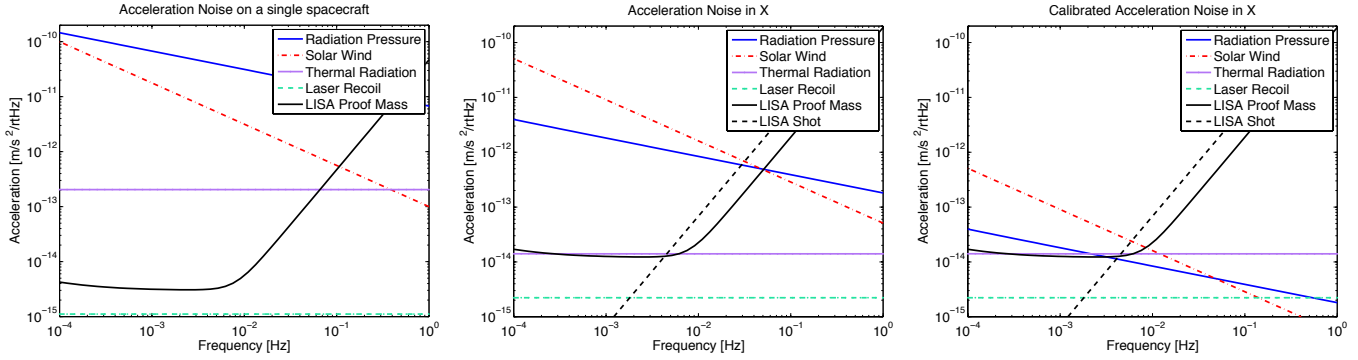


Figure 3: The acceleration noise for (left) a single spacecraft, (center) acceleration noise in the Michelson combination, X , and (right) the final noise in X after force noise subtraction.

levels between the single spacecraft acceleration and in X we see the solar radiation pressure and thermal radiation have significant reduction in couplings because of their large radial component. However, the solar wind pressure has smaller suppression because of its larger non-radial component (due to deviation of the solar wind from the radial direction). The calculation of the couplings, detailed in Appendix A, is entirely based on the geometry of the constellation and the direction of each force. The radial spacecraft acceleration noise from the end spacecraft couples into X with a suppression of factor of 100 compared with acceleration noise in the sensitive (transverse) direction. The suppression factor of the radial acceleration noise of the middle spacecraft is common to both interferometer arms and receives a factor of 500 suppression.

4.3 Force calibration and subtraction

By direct measurement of the solar wind and solar radiation, the resulting force on the spacecraft can be scaled and subtracted from the Michelson data. With current instruments, a factor of 100 of solar wind force and solar radiation pressure force appears to be achievable, though further investigation into solar wind calibration is needed. The calibrated acceleration noise budget shown in Figure 3 (right), is a factor of 20 higher than the LISA acceleration noise at $100\mu\text{Hz}$ and reduces at higher frequencies. The final acceleration noise in the Michelson can be approximated by $A_X \approx 5 \times 10^{-16} \times (1\text{Hz}/f)^{3/4} \text{ m/s}^2/\sqrt{\text{Hz}}$ and the resulting displacement noise is calculated by $X_{Accel} = \frac{A_X}{(2\pi f)^2} \text{ m}/\sqrt{\text{Hz}}$.

4.4 Expected Interferometer Strain

With acceleration noise of X_{Accel} in the Michelson combination and interferometer measurement system noise of X_{IMS} in the Michelson combination, the sensitivity can be calculated as

$$h(f) = \frac{\sqrt{5}}{2} \frac{T(f)}{\sin(2\phi)} \frac{\sqrt{X_{Accel}(f)^2 + X_{IMS}(f)^2}}{(2\pi f)^2 L} \quad (2)$$

where $T(f)$ is the interferometer response to gravitational waves ¹. The interferometer response differs from LISA in two important ways: the arm length is longer lowering the corner frequency of the interferometer response to gravitational waves by a factor of 4, and the angle of the Michelson arms $2\phi = 164^\circ$ reduces the sensitivity to gravitational waves for fixed arm length by a factor of 3.

5 Mission Design and Alternatives

We propose a two year mission and use a less expensive launch vehicles, the SpaceX Falcon 9, expected to be available at launch time. Due to the lack of a drag free system, there are less stringent requirements for

¹ $T(f)^{-1} \approx \sqrt{1 + (f/(a_0 f_0))^2}$, with $f_0 = c/(2L) = 7\text{mHz}$ and $a_0 = 0.41$

thrusters than those planned by LISA. We baseline a smaller (20cm diameter telescope) to further reduce the spacecraft size and mass, while the relatively small change of the Michelson vertex angle over the mission lifetime ($\pm 0.15^\circ$) allows the telescope actuation system required for LISA to be replaced with in-field guiding - actuation of the telescope secondary or other optical element smaller than the primary.

5.1 Launch and Orbit Insertion

A detailed analysis of the possible spacecraft trajectories has not been completed, however based on SGO-Mid [9] and missions at $\mathcal{L}2$ we expect that achieving the required orbits is entirely feasible. The three S/C and propulsion modules will be launched on a single launch vehicle. One scenario could be all three S/C and prop-modules could travel to $\mathcal{L}2$ then, S/C 1 and S/C 3 could be allowed to follow the invariant manifolds to leave Earth and head for heliocentric orbits. S/C 3 can naturally depart $\mathcal{L}2$ and drift back to position. S/C 1 could travel from $\mathcal{L}2$ to $\mathcal{L}1$ which costs very little fuel ($\Delta V \lesssim 1$ m/s) but will take about 6 months, then to depart $\mathcal{L}1$ and head for its final location 8° in front of the Earth. Once S/C 1 and S/C 3 reach their respective heliocentric locations, they need to perform a maneuver to insert into their final orbits.

5.2 Orbits

The orbits are designed to maintain the constellation for as long as possible with minimal station keeping. The parameters of the constellation plotted in Figure 4 show that reasonable range-rate and range can be maintained for the nominal 2 year mission. Minor station keeping maneuvers are required 4-6 times per year to maintain S/C 2 orbit about $\mathcal{L}2$. We have assumed no station keeping for S/C 1 or S/C 3. With the initial velocities set in this orbit simulation, all mission parameters are upheld for almost 2 years (geometric suppression drops below 100 after 630 days). With optimization, we expect all orbital mission parameters described in Table 1 could be met for 2 years.

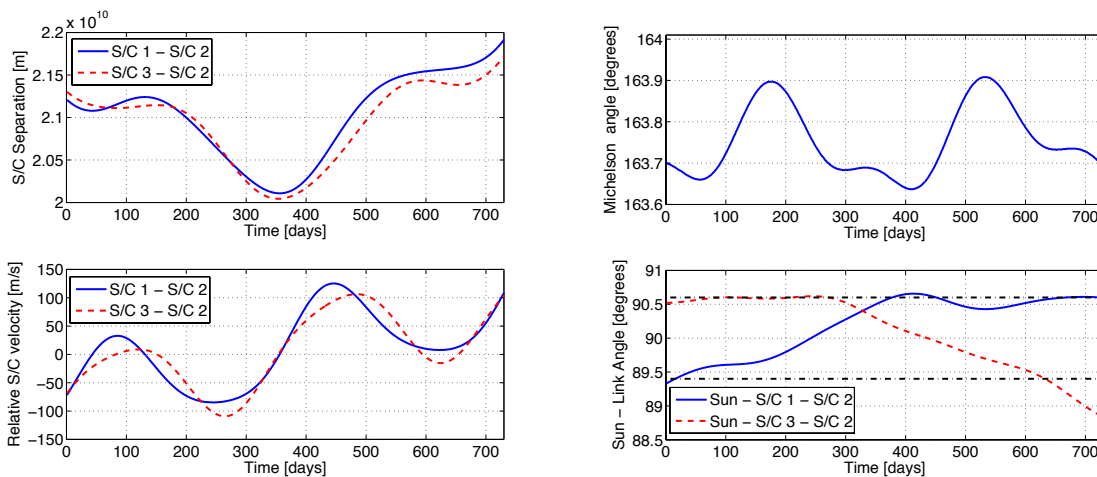


Figure 4: Left: The S/C separation (top) and relative velocity (bottom). Right: The Michelson internal angle (top) and and the angle of the interferometer link to the Suns radial direction (bottom). Values between dashed lines give a geometric suppression factor of 100, or more.

5.3 Work to go

The LAGRANGE mission presented here is a plausible implementation of the geometric suppression of spacecraft noise based on our extensive experience with LISA, gravity sensing, and solar sensing. While every attempt has been made to give a reasonable values the time and rigor required for mission design optimization has not been applied. Specific items that can be explored to optimize the science per dollar and balance risk against performance are addressed in Table 3.

Although LAGRANGE affords many technical and operational simplifications compared with LISA, it has increased demands on some subsystems introducing some new risks. Experience with LISA technology development leave us confident that the reduction in received optical power by 250 times and the six-fold increase in Doppler shifts (up to 120 m/s) can be accommodated with minor modification to existing technologies. Removal of the GRS does require tight knowledge or control of non-gravitational forces including thermal re-radiation and outgassing (preliminary outgassing analysis shows fluctuations should be below $10^{-15} \text{m/s}^2/\sqrt{\text{Hz}}$ in the sensitive direction of the interferometer). Additional verification of the performance of solar wind monitors would reinforce the viability of the calibration approach.

Table 3: Mission alternatives

Trade	Notes
4 interferometer links versus 6	Added links may have degraded performance but might provide better science per dollar
Attitude control with reaction wheels and hydrozene thrusters vs. alternate (eg micro- or milli-Newton thruster)	Performance versus mass/power/cost/maturity
Separate prop module vs. integrated prop system	Cost and complexity versus performance. Additional mass during science improves performance; gravity gradients not an issue
Freely evolving orbits vs. periodic stationkeeping maneuvers	Current orbits are life limiting
Telescope size and laser power	Design optimization to ensure robust received signal and avoid driving spacecraft and optical cost
Data volume/rate vs telecom resources	Science requirements only go up to 0.1 Hz, but LISA system supported 1 Hz measurements.
Orbiter mass	Higher mass improves science performance, so extra mass is desirable as supported by the Launcher
Accelerometer vs no accelerometer	Accelerometer not strictly needed for science return but viewed as valuable diagnostic

5.4 Cost estimate

The cost information contained in this document is of a budgetary and planning nature and is intended for informational purposes only. It does not constitute a commitment on the part of JPL and/or Caltech. The accuracy of the estimate is commensurate with the level of understanding of a Pre-Phase A mission concept.

The LAGRANGE mission, Phases A-F cost estimate is \$1.1 Billion (FY12). This estimate is based on the \$1.4 Billion (FY12) GSFC Space Gravitational Observatory - Mid (SGO-Mid) concept [9] given the many similarities with SGO-Mid, the high level of detail of the SGO-Mid cost estimate, and the maturity of SGO-Mid concepts. Similarities between SGO-Mid and LAGRANGE include: three spacecraft, high precision inter-spacecraft interferometry, mission lifetime (2 years science operation), orbit insertion points (SGO-Mid is 9 degrees Earth trailing, while this mission has spacecraft 8 degrees Earth leading/trailing), and deep space communications for data retrieval. Major cost differences between the SGO-Mid and LAGRANGE are attributed to differences in the hardware and shown in Table 4. Additional savings could be expected since LAGRANGE requires a smaller and lighter spacecraft.

Breakdown of cost differences: The LAGRANGE estimate was prepared without consideration of potential industry participation and derived using a combination of parametric mass-based cost models and adjustments to the SGO-Mid cost estimate for design differences. The cost models provide only the total development cost for the first flight unit. Subsequent units are estimated using the following learning curve assumption of N total units: total cost = single unit cost $\times 5(1 - (0.8)^N)$.

Acknowledgments: We gladly acknowledge: Jeff Livas, Tuck Stebbins and the SGO core team for detailed discussion on the SGO missions and mission cost; Min-Kun Chung, Ted Sweetser and Martin Lo for spacecraft orbit modeling.

6 References and Citations

- [1] P. Bender and K. Danzmann, and the LISA Study Team, Doc. MPQ 233 (1998).
- [2] Y. Chen and S. Kawamura, Phys. Rev. Lett. 96, 231102 (2006)
- [3] W. M. Folkner, A non-drag free gravitational wave detector. Private communications 2008; W. M. Folkner, "A non-drag-free gravitational wave mission architecture", Concepts for the NASA Gravitational-Wave Mission, call (NNH11ZDA019L) (2011).
- [4] D. J. McComas, S. J. Bame, P. Barker, W. C. Feldman, J. L. Phillips, P. Riley, and J. W. Griffiee, Space Science Reviews, 563 **86** (1998); <http://faesr.ucar.edu/view/835>, <http://swepam.lanl.gov/>
- [5] E. C. Stone, A. M. Frandsen, R. A. Mewaldt, E. R. Christian, D. Margolies, J. F. Ormes, and F. Snow, Space Science Reviews, 1, **86** (1998); <http://www.srl.caltech.edu/ACE/>
- [6] T. Appourchaux, B. N. Andersen, C. Frohlich, A. Jimenez, U. Telljohann, and C. Wehrli, Solar Physics **170** 27, (1997).
- [7] C. Frohlich, J. Romero, H. Roth, et al. Solar Physics, 101 **162**, (1995).
- [8] Astro2010: The Astronomy and Astrophysics Decadal Survey http://sites.nationalacademies.org/bpa/BPA_049810
- [9] Space Gravitational Observatory - Mid (SGO-Mid) concept. Submitted to concepts for the NASA Gravitational-Wave Mission, call (NNH11ZDA019L) (2011).
- [10] Gijs Nelemans, Class. Quantum Grav. 094030 **26** (2009).
- [11] B. S. Sheard, M. B. Gray, D. E. McClelland, and D. A. Shaddock, Phys. Lett. A 320, 9 (2003).
- [12] J. W. Armstrong, F. B. Estabrook, and M. Tinto, ApJ **527** 814 (1999)
- [13] G. de Vine, B. Ware, K. McKenzie, R. E. Spero, W. M. Klipstein, and D. A. Shaddock Phys. Rev. Lett. **104**, 211103 (2010).
- [14] The LISA Frequency Control White Paper, D. A. Shaddock, et al. ESA document LISA-JPL-TN-823, (2009).
- [15] K. McKenzie, R. E. Spero, and D. A. Shaddock Phys. Rev. D **80** 102003 (2009)
- [16] J. I. Thorpe, P. Maghami, J. Livas, Phys. Rev. D **83** 122002 (2011)
- [17] Bonny L. Schumaker, *LISA's Disturbance Reduction System* Lecture, Caltech Physics Course 2002.
- [18] H. Peabody, S. Merkwitz, *LISA Thermal Design* 5th LISA Symposium (2004)
- [19] J.-P. Marque, B. Christophe, F. Liorzou, G. Bodoville, B. Foulon, J. Guerard, V. Lebat, Document IAC-08-B1.3.7 <http://www.onera.fr/dmph/goce/IAC-08-B1.3.7.pdf>
- [20] S.V.Dhurandhar, K.R.Nayak, and J.-Y.Vinet, Phys. Rev. D 65, 102002 (2002).
- [21] H-R. Schulte M. Herz, LISA Measurement Performance, LISA EADS Astrium LISA Mission Formulation Technical Note LISA-ASD-TN-1002 0.7 (2007)
- [22] D A Shaddock 2008 Class. Quantum Grav. 25 114012 (2008)
- [23] V.V. Beletskii, Motion of an Artificial Satellite About Its Center of Mass, Mechanics of Space Flight (1966).
- [24] Spacecraft attitude determination and control, Edited by J. R. Wertz, Astrophysics and Space Science Library, Dordrecht: Reidel (1978)
- [25] D. A. Shaddock, M. Tinto, F. B. Estabrook, and J. W. Armstrong, Phys. Rev. D **68**, 061303 (2003)

A Geometric suppression of noise

We now calculate the coupling of acceleration noise into the interferometer using the geometry described in Figure 1. We start by defining a coordinate system in Figure 5 where the unit vector \hat{y} describes the direction radially away from the Sun in line with the Earth, and \hat{x} is at right angles to \hat{y} in the plane of the ecliptic. For simplicity, we consider only motions in two (\hat{x}, \hat{y}) dimensions, with the \hat{z} completing the right angle triad being neglected. The radial, \hat{r}_j and transverse, \hat{t}_j unit vectors for the j th spacecraft can be transformed into the \hat{x}, \hat{y} coordinates through the rotation matrix:

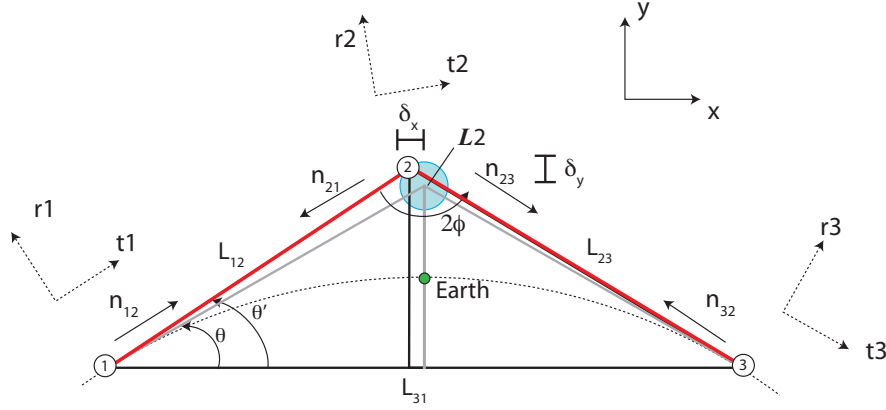


Figure 5: Spacecraft constellation geometry used to calculate the geometric suppression of spacecraft noise.

$$\begin{pmatrix} \hat{t}_j \\ \hat{r}_j \end{pmatrix} = \mathcal{R}(\zeta_j) \begin{pmatrix} \hat{x} \\ \hat{y} \end{pmatrix} \quad (3)$$

where the rotation matrix is given by

$$\mathcal{R}(\zeta_j) = \begin{pmatrix} \cos \zeta_j & \sin \zeta_j \\ -\sin \zeta_j & \cos \zeta_j \end{pmatrix} \quad (4)$$

and the angles of the three spacecraft relative to the \hat{x}, \hat{y} coordinates are $\zeta_1 = \theta$, $\zeta_3 = -\theta$, and $\zeta_2 = \beta$. The unit vectors defining the sensitive axis for each interferometer link are

$$\hat{n}_{12} = -\hat{n}_{21} = -\cos \theta^{(1)} \hat{x} - \sin \theta^{(1)} \hat{y} \quad (5)$$

$$\hat{n}_{32} = -\hat{n}_{23} = \cos \theta^{(3)} \hat{x} - \sin \theta^{(3)} \hat{y} \quad (6)$$

where $\theta^{(1)}$ ($\theta^{(3)}$) describes the angle from the \hat{x} axis to the interferometer link between spacecraft 1 (3) and spacecraft 2.

$$\tan \theta^{(1),(3)} = \frac{L_{AU}(1 - \cos \theta) + L_{L2}}{L_{13}/2 \mp \delta} \quad (7)$$

where the minus sign in the denominator goes with $\theta^{(1)}$ and the plus with $\theta^{(3)}$ and $L_{AU} = 1.5 \times 10^{11}m$. It is natural decompose many spacecraft disturbances into radial and transverse components

$$\mathbf{a}_{Kj} = \begin{pmatrix} a_{Kj|R} \\ a_{Kj|T} \end{pmatrix} \quad (8)$$

For the K th noise source. The acceleration noise of the j th spacecraft projected onto the i th interferometer link with unit vector \hat{n}_{ij} is a function of geometry

$$a_{ij} = \left[\mathcal{R}(\zeta_j) \begin{pmatrix} \hat{x} \\ \hat{y} \end{pmatrix} \right]^T \mathbf{M} \mathbf{a}_{Kj} \cdot \hat{n}_{ij} + a_{Oij} \quad (9)$$

where \mathbf{M} is a 2×2 matrix that describes the coupling of the acceleration noise components \mathbf{a}_{Kj} into the radial and transverse directions \hat{r}_j, \hat{t}_j . \mathbf{M} takes cross coupling into account with off diagonal components ϵ_T and ϵ_R .

$$\mathbf{M} = \begin{pmatrix} 1 & \epsilon_T \\ \epsilon_R & 1 \end{pmatrix}. \quad (10)$$

With $\epsilon_R = \frac{1}{fT}$, and T the period of the Earth Orbit about the Sun. ϵ_R factors in the transverse-orbital coupling imposed by fluctuating radial forces, while $\epsilon_T \approx 0$. The term a_{Oij} in Equation 9 describes other interferometer noise sources, such as shot noise, that do not have a geometric interpretation. The Michelson interferometer combination with spacecraft 2 at the vertex can be made up of one way links as $X = [s_{12} + D_{12}s_{21}] - [s_{32} + D_{23}s_{23}]$ [25]. If we consider only the acceleration noise in X and approximate the delays of the arms to be equal ($D_{ij} = D$) we can find the acceleration noise in the Michelson combination

$$\begin{aligned} A_X &= (1 + D^2)(a_{12} - a_{32}) + 2D(a_{21} - a_{23}) \\ &= (1 + D^2)(C_{R2}a_{R2} + C_{T2}a_{T2}) + 2D(C_{R1}a_{R1} + C_{T1}a_{T1} + C_{R3}a_{R3} + C_{T3}a_{T3}) \end{aligned} \quad (11)$$

where a_{Ri}, a_{Ti} are the radial and transverse accelerations on each spacecraft are²

$$a_{Ri} = \sqrt{a_{RP|Ri}^2 + a_{SW|Ri}^2 + a_{Th|Ri}^2 + a_{LF|Ri}^2 + a_{IR|Ri}^2}, \quad (12)$$

$$a_{Ti} = \sqrt{a_{RP|Ti}^2 + a_{SW|Ti}^2 + a_{Th|Ti}^2 + a_{LF|Ti}^2 + a_{IR|Ti}^2} \quad (13)$$

The geometric coupling factors are

$$C_{R1} = 2 \sin(\theta_1 - \theta^{(1)}) + \epsilon_R \quad (14)$$

$$C_{T1} = 2 \cos(\theta_1 - \theta^{(1)}) \quad (15)$$

$$C_{R2} = 2(\sin(\beta - \theta^{(1)}) + \sin(\beta + \theta^{(3)})) + \epsilon_R \quad (16)$$

$$C_{T2} = 2(\cos(\beta + \theta^{(3)}) + \cos(\beta - \theta^{(1)})) \quad (17)$$

$$C_{R3} = -2 \sin(\theta_3 - \theta^{(3)}) + \epsilon_R \quad (18)$$

$$C_{T3} = -2 \cos(\theta_3 - \theta^{(3)}) \quad (19)$$

Note that we assume no correlations between the noise on the different spacecraft. The geometric coupling factors reveal the geometric suppression of radial acceleration noise:

$$C_{T1} = 2.00, \quad C_{T2} = 3.95, \quad C_{T3} = 2.00, \quad C_{R1} = 0.02, \quad C_{R2} = 0.007, \quad C_{R3} = 0.02 \quad (20)$$

This shows the coupling of transverse spacecraft acceleration into the Michelson combination is twice the transverse acceleration noise for the end spacecraft, and four times the transverse spacecraft acceleration for the center spacecraft. On the other hand, the radial spacecraft acceleration noise coupling into the Michelson combination is 1/100th that of transverse noise for the end spacecraft and approximately 1/500th for the middle spacecraft. The acceleration noise budget for the Michelson combination, X , is shown in Figure 3 (center). Here, we see that the radiation pressure and thermal noise have significant reduction in couplings because their radial component, while the solar wind has a larger transverse component which arises due to deviation of the solar wind from the radial direction.

²For simplicity radial and transverse components of acceleration noise are assumed to be independent. This is not accurate but doesn't effect the outcome significantly here.

B Solar wind force and calibration

B.1 Force due to solar wind

The force due to the solar wind is dominated by ions, which can be modeled by an elastic impact without reflection [23]. The particle energies are generally completely absorbed, then the particles escape with only thermal velocity equal to that of the surface molecules [24]. The force delivered by the wind with velocity relative to the spacecraft, v and direction unit vector $\hat{\mathbf{v}}$ (see Figure 6) is given by

$$\mathbf{F}_{\text{sw}}(f) = -\rho v^2 A (\hat{\mathbf{N}} \cdot \hat{\mathbf{v}}) \hat{\mathbf{v}} \quad (21)$$

where the density is ρ . To estimate $\mathbf{F}_{\text{sw}}(f)$ we used three years of data (2007, 2008, 2009) from the SWEPAM [4] instrument on the Advanced Composition Explorer mission [5]. We estimate the magnitude of the solar wind acceleration to be $a_{\text{sw}}(f) = 10^{-13} (1\text{Hz}/f)^{3/4} \text{m/s}^2 / \sqrt{\text{Hz}}$ with a approximately Gaussian distribution in the direction of the solar wind with a zero mean (about radial) and standard deviation of 3 degrees.

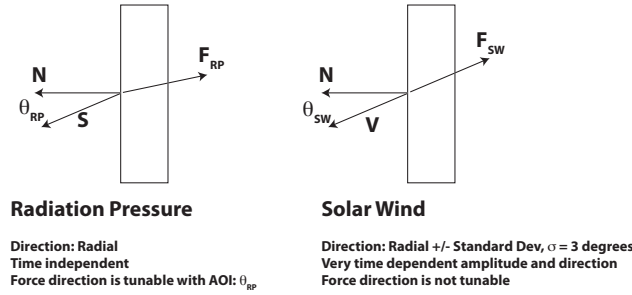


Figure 6: Direction of force for radiation pressure and solar wind. $\hat{\mathbf{N}}$ is a unit vector normal to the spacecraft face, $\hat{\mathbf{S}}$ is the unit vector from the spacecraft to the Sun and $\hat{\mathbf{V}}$ is the unit vector of the Solar wind velocity relative to the spacecraft.

B.2 Solar wind measurement precision

The solar wind pressure is $P = \frac{1}{2} \rho v^2$. The resulting radial and transverse accelerations are respectively

$$a_R = \frac{PA \cos \theta_{\text{SW}}}{m}, \quad (22)$$

$$a_T = \frac{PA \sin \theta_{\text{SW}}}{m}, \quad (23)$$

where A is the area of the of the spacecraft surface that faces the sun, m is the spacecraft mass, and θ_{SW} is the angle between the surface normal and the direction to the sun. We approximate $\cos \theta_{\text{SW}} = 1$ and $\sin \theta_{\text{SW}} = \theta_{\text{SW}}$. The acceleration noise spectrum in the (sensitive) transverse direction is

$$\tilde{a}_T = \frac{A}{m} \left(\tilde{P}(f) \theta_{\text{SWrms}} + P_{\text{rms}} \tilde{\theta}_{\text{SW}}(f) \right) = \tilde{a}_R(f) \theta_{\text{SWrms}} + a_{\text{rms}} \tilde{\theta}_{\text{SW}}(f). \quad (24)$$

where the rms subscript indicates root-mean-square average.

If the direction of the solar wind θ_{SW} changes slowly compared to gravitational-wave signal frequency f , then a_R will be well-correlated with gravitational-wave signal noise arising from the solar wind, and there is no need to explicitly measure a_T or θ_{SW} . That is, the second term in Equation 24 can be neglected, and the residual acceleration noise from the solar wind is given by the measurement noise in the radial acceleration measurement multiplied by θ_{SWrms} . If, on the other hand, the acceleration in the transverse direction is uncorrelated to the noise in the radial direction, or equivalently the angle is changing rapidly compared to signal frequency f , then the suppression of the solar wind-induced acceleration is the noise in the angle measurement $\tilde{\theta}_{\text{SWrms}}$, and

it will be necessary to measure this quantity with high precision. Further study of the properties of the solar wind are needed to know which case applies. If high-precision measurements of θ_{SW} are necessary, this can be implemented with two monitors, one in the radial direction and one in the sensitive direction with approximately 10 times higher gain.

C Costing detail

Table 4: Cost Estimate (\$M FY12)

Cost Differences between SGO-Mid and LAGRANGE	Cost (FY12\$M)
GSFC Space Gravitational Observatory - Mid (SGO-Mid)	1,400
Gravitational Reference System: \$196M cost reduction for removing six GRS units. A single GRS is estimated at \$53M using a parametric mass-based modeling tool. This estimate aligns with the SGO-Mid estimate of \$50 Million, which is used as a basis for the six-unit reduction.	(196)
Two telescope assemblies and optical benches: \$90M cost reduction. (LAGRANGE requires 4; SGO-Mid requires 6). Removal of laser pre-stabilization on each spacecraft:\$15M	(105)
Solar Wind Monitor: \$17M cost increase for three additional units. A single solar wind monitor is estimated at \$7M using a parametric mass-based modeling tool and is the basis for the two-unit increase.	17
Radiometer: \$17M cost increase for adding three units. A single radiometer is estimated at \$7M using a parametric mass-based modeling tool and is the basis for building three-units.	17
Accelerometer: \$13M cost increase for adding three units. Estimated for GRACE.	13
Attitude Control: \$40M cost savings due to a different ACS design. SGO-Mid uses Micro-Newton thrusters, whereas this mission uses reaction wheels and desaturation thrusters. An estimate of the total cost of colloidal thrusters for LISA is \$80 Million, while an estimate for the total cost of hydrazine thrusters and reaction wheels on this mission is \$40 Million.	(40)
Laser Power: \$10M cost increase due to the 1.2 Watt higher power (LISA-like) laser compared to the SGO-Mid 0.7 Watt laser.	10
LAGRANGE	1116

D Team member information

Contributor	Email
Kirk McKenzie ¹	kirk.mckenzie@jpl.nasa.gov, (818) 235 8358
Robert E. Spero ¹	spero@jpl.nasa.gov
William M. Klipstein ¹	klipstein@jpl.nasa.gov
Glenn de Vine ¹	Glenn.devine@jpl.nasa.gov
Brent Ware ¹	Brent.Ware@jpl.nasa.gov
Michele Vallisneri ¹	Michele.Vallisneri@jpl.nasa.gov
Curt Cutler ¹	Curt.J.Cutler@jpl.nasa.gov
John Ziemer ¹	John.K.Ziemer@jpl.nasa.gov
Daniel A. Shaddock ²	daniel.shaddock@anu.edu.au
Ruth Skoug ³	rskoug@lanl.gov
John Steinberg ³	jsteinberg@lanl.gov
1. Jet Propulsion Laboratory, California Institute of Technology, Pasadena, California 2. Department of Physics, The Australian National University, Canberra, Australia 3. Los Alamos National Laboratory, Los Alamos, New Mexico	